

# Estimation of absorbed fraction and specific energy of radon progeny for a Syrian adult tracheobronchial tree

B. Rawaa\* and S. Al Tarabichi

Physics Department, Faculty of Science, Damascus University, Syria

## ABSTRACT

**Background:** Ongoing Estimating the health effect of  $^{222}\text{Rn}$  progeny deposited on inner surfaces of airways regions is of great interest because  $^{222}\text{Rn}$  progeny are considered the major contributors in imparted energy to lung structures. **Materials and Methods:** In this study, (CT) scan of a healthy, non-smoking Syrian volunteer male, 3D-Slicer 4.7.0 medical image processing software, Solidworks mechanical design software and MCNPX 2.5.B code were used to create the geometry and to evaluate the absorbed fraction and specific energy due to alpha particles emitted by inhaled radon progeny in nuclei and layers of sensitive cells in the epithelium of human tracheobronchial tree. Absorbed fraction (AF) and specific energy were determined using Micro-dosimetry approach and airway tube wall as proposed by ICRP (1994), and NRC (1991). **Results:** Absorbed fractions (AFs) and specific energy of alpha particles were calculated for each generation from 1st to 15th. Comparison of average AFs values in sensitive layers was carried out with ICRP66 airway model where some significant differences were found due to dimensions differences between both models. Furthermore, AFs of cell nuclei had the same trend of those for layers, where the highest values were for 7.69 MeV alpha particles in BB region and the opposite in bb region. **Conclusion:** Interactions of alpha particles with secretory and basal cells show significant differences which can influence dose weightings. Comparisons with ICRP66 data reveal the influence of geometry and target cells distribution on absorbed fraction and specific energy values.

**Keywords:** Absorbed fraction, specific energy, Radon progeny, micro-dosimetry; Monte Carlo method.

## ► Original article

### \*Corresponding authors:

Bardan Rawaa, PhD.,

### E-mail:

[baradan.raw@gmail.com](mailto:baradan.raw@gmail.com)

Revised: February 2018

Accepted: June 2018

Int. J. Radiat. Res., October 2019;  
17(4): 605-615

DOI: 10.18869/acadpub.ijrr.17.3.605

## INTRODUCTION

Inhalation of the short-lived radon progeny ( $^{218}\text{Po}$ ,  $^{214}\text{Pb}$ ,  $^{214}\text{Bi}/^{214}\text{Po}$ ) in homes, the outdoor atmosphere and at work places provides the largest fraction to the natural radiation exposure of population (1-3). Biological radiation induced effects in the lungs due to inhaled radon progeny are caused primarily by highly localized energy deposition of alpha particle tracks at the cellular level, where alpha emitted by radon progeny deposited on inner surfaces of airway tubes damage the radiosensitive target cells and give rise to pathological changes (4, 5). Dosimetric

modelling of the respiratory tract started soon after the Second World War in 1949 in relation to the enhanced necessity for nuclear technology and uranium ore exploring. The needs for standardization of values for parameters describing inhalation, deposition, retention and translocation of airborne radionuclides in workers for the purpose of deriving exposure limits (6).

In Human Respiratory Tract (HRT) model, secretory and basal cells in bronchial region BB and secretory cells in bronchiolar region bb are the main targets because of their alpha particles' sensitivity. Calculation of the dose absorbed in

sensitive targets has been a subject of many studies such as ICRP66<sup>(5,7,8)</sup>, where in their dosimetric approach, dose is calculated in layers containing the sensitive cells by assuming that values in sensitive cells are the same as those in layers. Such an approach did not consider details of sensitive cells in layers.

Another possible approach is the Micro-dosimetric method<sup>(9-11)</sup>, which calculates distributions of Micro-dosimetric quantities in human lung. Number of Micro-dosimetric models have been developed in the past<sup>(5,12)</sup>. Such models are, the Track Structure Model<sup>(13,14)</sup>, the Threshold Specific Energy Model<sup>(15)</sup> and LET model<sup>(16)</sup> derived from cellular irradiation experiments. On the other hand, Micro-dosimetric parameters have also been computed by different approaches based on analytical and Monte Carlo techniques<sup>(17-20)</sup>.

Nikezic et al.<sup>(9,21)</sup> replaced calculations of absorbed energy in layers by calculations of absorbed energy in spherical and ellipsoids cell nuclei using a written Fortran program, namely, FORMING to distribute cell nuclei in airway tube wall. Hofmann et al.<sup>(10)</sup> also used spherical cell nuclei to calculate the LET spectra for radon progeny under the bifurcation and cylindrical geometry and to study the effects of non-uniform deposition of radon progeny on absorbed dose.

Due to the lack of detailed human respiratory model for the Middle East region and the complex of MCNP input file structure where the description of complex geometric model is highly abstract and error-prone, this work aims at constructing a model of respiratory airways for a Syrian adult man, using the computing software power to build airway tube model (input files that correspond to CAD model) with a large number of sensitive cells nuclei which exploited in evaluating Micro-dosimetric quantities, such as, absorbed energy fraction and specific energy of alpha particles emitted by radon progeny in nuclei and layers of sensitive cells in airway tube wall as proposed by ICRP (1994)<sup>(7)</sup>, and NRC (1991)<sup>(22)</sup> for radiation protection and medical purposes.

The present work is the first research that investigates the anatomy of human respiratory

system in the Arab region, where most of relevant studies depend on anatomical dimensions according to ICRP66 model or dimensions of the most important models in published literature.

## **MATERIALS AND METHODS**

### **CT data**

The geometry of human airways was obtained from computed tomography (CT) scan of a healthy, non-smoking volunteer male his anatomical data (33 years old, 75 kg weight, 172 cm height)<sup>(23)</sup>. The examination was performed with Siemens scanner Somatom Sensation 64 at 120 kVp. The total number of slices was 500 each of 3 mm thickness, consisted of a matrix of 512×512 pixels. The plan resolution is 1.024 pixel in each millimetre, therefore, the voxel size is 0.4×0.4×3 mm<sup>3</sup><sup>(23)</sup>, and only 96 slices contained the anatomical structure of respiratory airways were used in this study.

The interest axial CT-scan images (DICOM files) were transformed to the 3D-Slicer 4.7.0<sup>(24)</sup> which is a strong medical image processing software for three-dimensional reconstructions. The measurements of the central airways were made by the same person.

Tracheal diameter, tracheal cross-sectional area, diameter and length of right and left main bronchus, right and left lobar bronchus and branching angle of lobar bronchi from their main bronchus and branching angle of lobar bronchi between each other were measured. Then, respiratory airways were segmented manually with the help of radiologist and using human's anatomy atlases to define the required boundaries where, a 3D airways model was constructed and transferred in Standard Tessellation Language (STL) format to Solidworks 15.0 mechanical design and simulation software<sup>(25)</sup> as shown in figure 1. The final model was started from the inlet of trachea and the longest detected airway extended to nine generation.

Because of their anatomic location, some bronchus cannot be evaluated accurately in CT slices. Therefore, they were evaluated using

Solidworks measurement tool.

Morphological data suggest that in proximal regions, where the lung follows a complete dichotomous branching scheme, the average diameters and lengths of successive airways correspond to each other as <sup>(26)</sup>.

$$D_{i+1}=D_i 2^{-1/3} \quad L_{i+1}=L_i 2^{-1/3}$$

where  $D_i$  and  $L_i$  are the diameter and length of the tube that converge into the duct of diameter and length  $D_{i+1}$  and  $L_{i+1}$ , respectively. The previous relations were used to determine dimensions of the rest airways. All measured and calculated dimensions were listed in table 1.

Dimensions in table 1 were averaged and compared with literature morphometry models. These models were the Weibel symmetrical model (Weibel, 1963), the Yeh-Schum asymmetrical model (Yeh & Schum, 1980), and the ICRP66 symmetrical model (ICRP, 1994) <sup>(26)</sup>. The dimensions of airway tubes of the three models were listed in table 2.

### Location of target cell nuclei

As mentioned before, the morphometry model of a Syrian man is used in this study. Before the simulations could be carried out, the locations of target cell nuclei in sensitive layers need to be identified. Distributions of Target cells proposed by ICRP66 <sup>(7)</sup> and NRC <sup>(22)</sup> have been adopted, where in bronchial (BB) region (generations 1 to 8), both basal and secretory cells are target cells.

According to ICRP66 and NRC the airway tube wall in BB region comprises 5 $\mu$ m of mucus, 6  $\mu$ m of cilia and fluid, 30  $\mu$ m of a layer containing secretory cells, and 15  $\mu$ m of a layer containing basal cells. Basal cells are distributed between 35 and 50  $\mu$ m below the epithelial surface and secretory cells are distributed between 10 and 40  $\mu$ m below the surface <sup>(21,22)</sup>. According to ICRP66 and NRC the tube wall in bb region comprises 2 $\mu$ m of mucus, 4 $\mu$ m of cilia and fluid, and 8  $\mu$ m of a layer with secretory cells <sup>(9)</sup>. Secretory cells are distributed between 4 and 12  $\mu$ m below the epithelial surface <sup>(21)</sup>.

It is clear that the nuclei of sensitive cells occupy only a relatively small volumetric

fraction of the layer, so only a relatively small proportion of cell nuclei is hit by alpha particles, and the majority of the cells do not receive any dose and will remain intact. In other words, most alpha particles miss sensitive targets and dissipate their energies in the insensitive tissue in the layer containing sensitive cells <sup>(9)</sup>. The average abundances of cell nuclei in the bronchial and bronchiolar wall were given by Mercer *et al.* <sup>(8, 27, 28)</sup>, where six categories of epithelium cells were defined and the most radiosensitive cells (secretory and basal) were studied in this work.

The product of the volume of the layer containing the sensitive cell nuclei and the volume abundance of the sensitive cell nuclei is divided by the volume of one nucleus to give the number of sensitive cell nuclei in the interested layer.

In our study, for practical purposes we simplify the description of the cell by considering that it consists of a central nucleus surrounded by cytoplasm. The geometry of the former is approximated by a sphere of 9  $\mu$ m diameter for secretory cell nuclei in BB and bb regions, of 8  $\mu$ m diameter for basal cell nuclei <sup>(9, 29)</sup>.

Each cell compartment is characterized by its atomic composition and density. The standard chemical composition for cell nucleus is provided by ICRU <sup>(30)</sup>, whereas cytoplasm composition was obtained by Byrne *et al.* <sup>(31)</sup> by subtracting the nucleus material from an average soft tissue corresponding values appear in table 3 <sup>(29)</sup>. In our study, mass density of nuclei and cytoplasm substances are taken to be 1 g.cm<sup>-3</sup> and 1.045 g.cm<sup>-3</sup>, respectively.

### MCNPX code and simulation

The Monte Carlo (MC) technique is a statistical method employing random numbers to Simulate stochastic processes. The MC method is excellent for simulation of the stochastic Nature of ionising radiation, and its interaction with matter (radiation transport). Monte Carlo N-Particle extended (MCNPX), was developed at Los Alamos National Laboratory, USA. The MCNPX code uses input files consist of three blocks. The first block is the cell card, which defines geometric volumes, with

respective materials and densities. The second block is the surface card containing the geometric surfaces from which the volumes are created. The third one is the data card contains the physics and source cards, which in short defines the material, source geometry, particle type, kinetic energy, energy cut-off, direction of emitted particle, tallies, and other characteristics <sup>(32)</sup>. In this study, MCNPX code version 2.5.B <sup>(32)</sup> was used and the simulation process involved two phases:

### **MCNPX geometry**

A mathematical model of an airway tube containing cell nuclei has been developed for the simulations and calculations. Each generation in BB and bb regions was defined like a set of circular concentric cylinders (located in a 3-d coordinate system) with different ratios to represent air, mucus, cilia, secretory and basal layers for BB region and the same one for bb region except basal layer <sup>(2)</sup>.

In this study, Solidworks 15.0 software was used to model and distribute cell nuclei within the sensitive layers using circular pattern features in each particular airway tube.

According to the difference between secretory and basal cells distribution, each type was treated separately. Then, the final step format files were imported to Ansys software by Design Modeler to be exported in MCNP format <sup>(33)</sup>.

In the next step, the prototype files according to (MCNP) formula obtained from Ansys software were imported to MCNPX code. These input files include the coordinates of surfaces which represent both components of airway wall and sensitive cells nuclei. Macrobody Rectangular Parallelepiped (RPP) were used to construct parallel rectangles extending along airway tube at each of these nuclei positions, as shown in figure 2.

RPP1 represents the first universe to be filled with a second universe RPP2 containing sensitive cell nucleus. Then, materials, radioactive sources and sensitive target cells in secretory and basal layers have been defined to create the final input files. Figure 3 shows cell geometry used in MCNP simulation in the

present study, secretory cells nuclei were located at 25 and 40µm depth below the epithelial surface in BB region, and at 12 µm depth in bb region, while basal cells nuclei were located at 45µm depth below the epithelial surface.

### **Monte Carlo Simulation and calculation of absorbed fraction and specific energy**

Monte Carlo simulations of alpha particles transport for each particular generation are started here. To calculate energy absorbed fraction (AF) and specific energy, we have considered distributed deposit sources in the length of each one of the fifteenth generations. Alpha particles emitted by radon progeny were distributed in mucus and cilia layers homogeneously as a volumetric cylinder source in SDEF card of MCNPX input file, while starting point and direction for emission of alpha particles were sampled randomly.

Energies of 6 and 7.69 MeV for alpha particles from <sup>218</sup>Po and <sup>214</sup>Po, respectively were used for all cases. Trajectories of alpha particles were simulated in airway tubes (tissue + air) system and sufficient particle histories (NPS) were run to reduce the coefficients of variation in data to be less than 10%, where NPS was set to 10<sup>6</sup> particles for all cases.

The desired information from a Monte Carlo simulation is obtained by a tally, i.e. predefined algorithms that score the contribution for each particle. MCNP tallies are normalized to be per starting particle and are printed in the output. The tally \*F8 was used to obtain energy deposited in (MeV). Then the absorbed fraction was calculated as follows <sup>(34)</sup>:

$$AF(t \leftarrow s) = \frac{*F8}{E_0}$$

where \*F8 is the energy deposited in the target organ (t) in MeV as obtained from MCNPX simulations, E<sub>0</sub> is the initial energy of the particle in MeV, AF(t←s) is the absorbed fraction of energy in the target organ (t) derived from radiation emitted from source organ (s).

while F6 tally provides the specific energy in (Gy) and it is defined as the energy imparted to a medium per unit mass <sup>(34)</sup>.

$$Z = 1.6 \times 10^{-10} \times F6$$

Where  $1.6 \times 10^{-10}$  is a conversion factor in unit of Gy·g/MeV.

A total of 92 input files were run on a personal computer (Core (TM) i5 - CPU 1.70GHZ - 8.00GB RAM) to achieve the goals of this study.

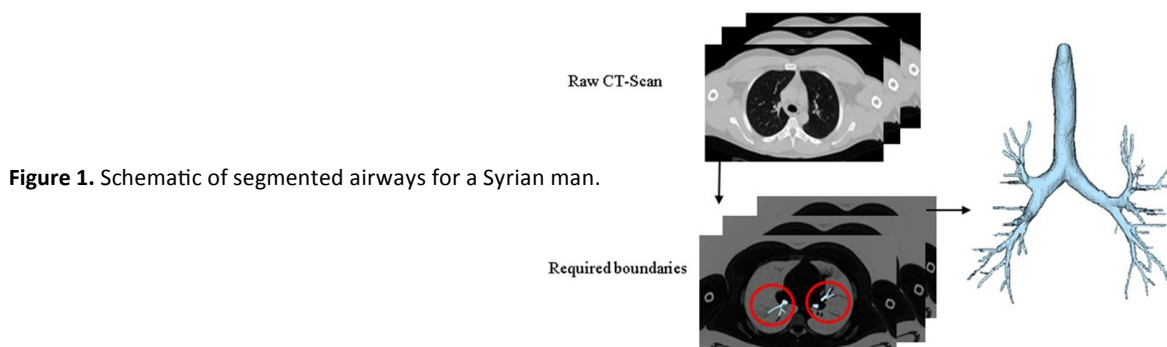


Table 1. Dimensions of TB- tree for a Syrian adult man.

Ge.NO	Right lobes						Left lobes				
	Upper		Middle		Lower		Upper		Lower		
	L	D	L	D	L	D	L	D	L	D	
0	8.79	1.82									
1	2.57	1.36					3.64	1.22			
2	2.30	0.83	3.42	1.10			2.01	0.71	3.01	1.01	
3	2.03	0.65	2.16	0.69	2.63	0.84	1.60	0.54	2.44	0.82	
4	1.66	0.53	1.81	0.58	2.37	0.76	0.93	0.31	2.18	0.73	
5	1.05	0.34	1.06	0.34	1.52	0.49	0.71	0.24	1.36	0.45	
6	0.89	0.29	0.89	0.29	1.04	0.33	0.41	0.14	0.55	0.18	
7	0.74	0.24	0.325	0.111	0.88	0.28	0.561	0.183	0.44	0.15	
8	0.11	0.33	0.258	0.088	0.70	0.23	0.445	0.145	0.33	0.11	
9	0.09	0.26	0.205	0.070	0.37	0.12	0.353	0.115	0.26	0.09	
10	0.071	0.206	0.163	0.056	0.294	0.095	0.280	0.091	0.370	0.120	
11	0.057	0.164	0.129	0.044	0.233	0.076	0.223	0.073	0.294	0.095	
12	0.045	0.130	0.103	0.035	0.185	0.060	0.177	0.058	0.233	0.076	
13	0.036	0.103	0.081	0.028	0.147	0.048	0.140	0.046	0.185	0.060	
14	0.028	0.082	0.065	0.022	0.117	0.038	0.111	0.036	0.147	0.048	
15	0.023	0.065	0.051	0.018	0.092	0.030	0.088	0.029	0.117	0.038	

L: length, D: Diameter; both in cm

Table 2. Average dimensions for Syrian man and literature models.

Ge.NO	Present study		Weibel		Yeh-Schum		ICRP66	
	L	D	L	D	L	D	L	D
0	8.79	1.82	12.0	1.8	10.0	2.01	9.1	1.65
1	3.11	1.29	4.76	1.22	4.36	1.57	3.8	1.2
2	2.69	0.913	1.9	0.83	1.78	1.133	1.5	0.85
3	2.17	0.708	0.76	0.56	1.27	0.846	0.83	0.61
4	1.79	0.582	1.27	0.45	1.17	0.678	0.9	0.44
5	1.14	0.372	1.07	0.35	1.24	0.570	0.81	0.36
6	0.76	0.246	0.90	0.28	1.03	0.459	0.66	0.29
7	0.59	0.193	0.76	0.23	0.88	0.370	0.60	0.24
8	0.37	0.181	0.64	0.186	0.78	0.307	0.53	0.2
9	0.26	0.131	0.54	0.154	0.66	0.259	0.437	0.165
10	0.24	0.114	0.46	0.13	0.56	0.217	0.362	0.135
11	0.19	0.090	0.39	0.109	0.43	0.164	0.301	0.109
12	0.15	0.072	0.33	0.095	0.34	0.120	0.25	0.088
13	0.12	0.057	0.27	0.082	0.25	0.090	0.207	0.072
14	0.09	0.045	0.23	0.074	0.19	0.069	0.17	0.06
15	0.07	0.036	0.20	0.066	0.16	0.045	0.138	0.053

L: length, D: Diameter; both in cm

**Table 3.** Chemical composition (in mass percentage) of cell nucleus<sup>(30)</sup> and cytoplasm<sup>(31)</sup>.

	H	O	C	N	P	Na	S	Cl	K
<b>Nucleus</b>	10.60	74.20	9.00	3.20	2.60	0.0	0.40	0.0	0.0
<b>Cytoplasm</b>	10.55	56.30	29.88	2.51	0.04	0.11	0.24	0.16	0.21

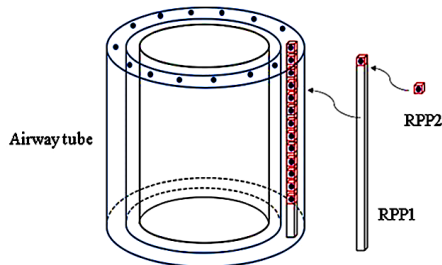


**Figure 2.** Geometrical model of airway and cells nuclei distribution.

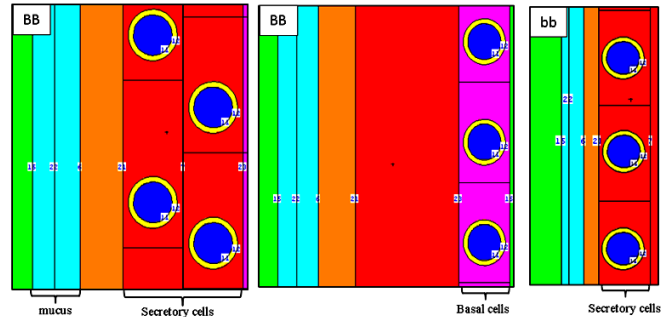


**Figure 3.** Schematic cell geometry used in MCNP simulation.

## RESULTS AND DISCUSSION

The simulations were performed by MCNPX code, for sources placed in various parts of BB and bb regions. Absorbed fraction (AF) and specific energy in sensitive cell nuclei and layers for alpha particles emitted from radon progeny were obtained.

### Absorbed fractions for target cell nuclei and layers

The results of AF are given in tables (4, 5 and 6) for secretory cell nuclei and layers in bifurcation region (BB), secretory cell nuclei and layers in bronchiolar region (bb) and basal cell nuclei and layers in bifurcation region (BB), respectively. ICRP66<sup>(7)</sup> average energy absorbed fraction values were added to the previous tables for easier comparison with similar layers values.

Results showed that AF values of target cell nuclei are small fraction of those for layers which contained sensitive cells for all studied cases and energies. Moreover, AF values increase with generation number despite the decrease in airway length due to the influence of the opposite (far) wall of the tube in calculations<sup>(35)</sup>.

Table 4 shows AF results for secretory cell nuclei and layers in bronchial region (BB). It can be observed that AF values for 7.69 MeV alpha

particles were higher than those for 6 MeV in BB region for fast and slow sources, while the opposite is true in bb region for both cell nuclei and layers as included in table 5.

AF values for 6 MeV alpha energy are well above those for 7.69 MeV, which can be explained by the decrease in the stopping power of alpha particles with the increase in their energies. Target cells in bb region are very close to alpha source therefore, alpha particles emitted with an initial energy of 6 MeV enter the sensitive layer with less energy in comparison with those of 7.69 MeV<sup>(36)</sup>.

The data of basal cells are given in table 6, where AF values from 7.69 MeV alpha particles have trends similar to those for secretory cells depending on generation number. AF values from 7.69 MeV were higher than AFs from 6 MeV for basal cells, where basal cells are more deeply embedded in the epithelium.

Comparisons with ICRP66 previous AFs data emphasized the fact that geometry and individual anatomy have an important effect on AFs, which are directly reflected on AF values for sensitive cell nuclei. ICRP66 considered the layers containing the target cells, i.e., the basal and secretory cells. Such an approach did not give values for particular generation or consider the structure, orientation, shape and abundance distribution of the sensitive cells in the layers. Furthermore, ICRP66 assumed infinitely long airway tubes with the most representative

diameter of 5 mm and 1 mm in BB and bb regions, respectively, <sup>(8,35)</sup>.

Inspection of these results reveal that in most cases, AFs from alpha particles emitted in the present study model are higher than ICRP66 values for secretory layers, while they are lower than ICRP66 values for basal layers.

### **Specific energy in target cell nuclei**

It is possible to estimate the average and the maximum specific energy, in a sensitive cell nucleus based on a simple assumption. If the diameter of the nucleus is 9  $\mu\text{m}$ , the volume and the mass of the nucleus are  $V=381 \mu\text{m}^3$  ( $381 \times 10^{-12} \text{cm}^3$ ), and  $m_N=1 \text{g.cm}^{-3} \times 381 \times 10^{-12} \text{cm}^3=381 \times 10^{-12} \text{g}$ , where  $\rho =1 \text{g.cm}^{-3}$  is the nucleus density.

Alpha particles with 7.69 MeV energy emitted by  $^{214}\text{Po}$  have a range of 71  $\mu\text{m}$  in tissue and their average stopping power is about 0.1  $\text{MeV}.\mu\text{m}^{-1}$ . This means that pathlength of alpha particles which cross the center of the nucleus is 9  $\mu\text{m}$ , and the energy imparted to the nucleus is about 1 MeV. Therefore, the corresponding specific energy is 1  $\text{MeV}/m_N=0.4 \text{Gy}$ .

Generally alpha particles do not cross the center, so the average specific energy should be smaller than 0.4 Gy. According to ICRU report 49 <sup>(30)</sup> the maximum stopping power of a particles in tissue is 0.24  $\text{MeV}.\mu\text{m}^{-1}$ . Hence, the maximum energy imparted to the cell nucleus and the maximum nucleus specific energy cannot be larger than 2.16 MeV and 0.9 Gy, respectively. Briefly, for the passage of a single alpha particle in the nucleus it is not expected to get a specific energy larger than 0.9 Gy.

In this work, specific energy was calculated for various combinations of alpha particle sources, energies and targets as shown in table 7 and 8 for BB and bb region, respectively.

Table 7 presents specific energy in sensitive cell nuclei of BB region for a single hit of alpha particle. It can be observed that alpha particles with initial energy of 7.69 MeV enter sensitive cell nuclei with larger energy than those particles with the initial energy of 6 MeV.

Furthermore, results illustrate how the nature of alpha particles interaction with cell nuclei changed with depth, where specific

energy for basal cell nuclei are lower than corresponding values for secretory cell nuclei in BB region. These results can be attributed to basal cell nuclei positions in airway tube, where they are deeper than secretory cell nuclei: basal cells are distributed at 45  $\mu\text{m}$  below the epithelial surface, while secretory cells are distributed between 25 and 40  $\mu\text{m}$  below the surface.

Moreover, the range of 6 MeV alpha particle in tissue is 48  $\mu\text{m}$ , and 71  $\mu\text{m}$  for the 7.69 MeV alpha particle. Therefore, if alpha particles with 6 MeV energy are emitted in BB fast mucus, the probability to hit a basal cell nucleus is very small, where basal cells are closed to the end of alpha particles range. Due to alpha particles short range, most of alpha particles lose their energies before reaching basal cells and this explains why the total absorbed doses in basal cell nuclei are lower than corresponding values for secretory cell nuclei.

Moreover, the specific location of alpha particles within the source layer affects the value of specific energy to epithelial cells. In this study a volumetric cylinder source was defined to present fast and slow mucus, so each point in these layers will act as a point radioactive source. Therefore, alpha particles deposited on bronchial airways are emitted from different positions in fast and slow mucus layers, where alpha particles emitted from the top of fast mucus layer will reach the epithelium with less energy than that emitted from the interface between fast mucus layer and the underlying slow mucus layer etc. <sup>(19,27,37)</sup>.

Table 8 shows specific energy values in sensitive cell nuclei of bb region, where higher values of specific energy from 6 MeV alpha particles were obtained in comparison with values of 7.69 MeV for fast and slow mucus sources. These results could be attributed to secretory cell nuclei position in bb region, where nuclei distributed at 12  $\mu\text{m}$  below the epithelial surface. Therefore, alpha particles with 6 MeV energy lose higher fraction of their initial energy, where alpha particles with 7.69 MeV still have enough energy to leave basal layer.

The specific energy in basal cell nuclei is significantly affected by their geometry.

Consequently, the basal cell doses were shifted to the lower dose range and they were much smaller than that in other references for 6 and 7.69 MeV alpha particles. These results were expected because basal cells are situated close to the end of the range of 6 MeV alpha particles as mentioned previously, where they situated at specific depth 12  $\mu\text{m}$  below the epithelium surface in the present study. Therefore, small energy transfer events were more probable for basal cells.

Moreover, specific energy values for secretory cells were relatively homogeneous

and results showed a proximity between specific energy values for secretory cells in the present study and references values, except of those for 6 MeV in BB region where lower values were obtained in this study.

In contrast, secretory cells suffer from more hits with large energy transfer which might be lethal and less efficient in cancer production. Since the dose in basal cells is much smaller than in secretory cells a heavier weighting for basal cell will bring down the calculated dose in the respiratory tract.

**Table 4.** Absorbed fraction for secretory cell nuclei and layers in BB region.

Source		Ge. No ↓	Layer		Nuclei	
			6 MeV	7.69 MeV	6 MeV	7.69 MeV
Fast mucus	This work	1	0.2333	0.3720	0.0573	0.0906
		2	0.2380	0.3799	0.0585	0.0922
		3	0.2407	0.3822	0.0585	0.0926
		4	0.2411	0.3831	0.0595	0.0933
		5	0.2423	0.3837	0.0599	0.0934
		6	0.2445	0.3832	0.0589	0.0925
		7	0.2437	0.3831	0.0597	0.0927
		8	0.2460	0.3846	0.0584	0.0919
		Mean	0.2412	0.3815	0.0588	0.0924
		ICRP66 →	0.249	0.353		
Slow mucus		Ge. NO ↓				
		1	0.2806	0.3890	0.0690	0.0942
		2	0.2832	0.3946	0.0695	0.0959
		3	0.2848	0.3969	0.0693	0.0958
		4	0.2857	0.3971	0.0695	0.0962
		5	0.2859	0.3974	0.0707	0.0967
		6	0.2902	0.3970	0.0690	0.0961
		7	0.2898	0.3445	0.0694	0.0832
		8	0.2922	0.3977	0.0684	0.0955
		Mean	0.2865	0.3893	0.0693	0.0942
ICRP66 →	0.272	0.355				

**Table 5.** Absorbed fraction for secretory cell nuclei and layers in bb region.

Source		Ge. No ↓	Layer		Nuclei		
			6 MeV	7.69 MeV	6 MeV	7.69 MeV	
Fast mucus	This work	9	0.2544	0.1914	0.0829	0.0624	
		10	0.2367	0.1865	0.0761	0.0600	
		11	0.2455	0.1897	0.0734	0.0577	
		12	0.2123	0.1662	0.0877	0.0686	
		13	0.2112	0.1643	0.0884	0.0689	
		14	0.2065	0.1594	0.0917	0.0707	
		15	0.2155	0.1641	0.0854	0.0653	
		Mean	0.2260	0.1745	0.0837	0.0648	
		ICRP66 →		0.214	0.172		
		Slow mucus		Ge. No ↓			
9	0.2680			0.1984	0.0873	0.0647	
10	0.2491			0.1931	0.0800	0.0621	
11	0.2529			0.1955	0.0769	0.0596	
12	0.2225			0.1713	0.0921	0.0708	
13	0.2211			0.1692	0.0923	0.0709	
14	0.2151			0.1637	0.0955	0.0728	
15	0.2239			0.1691	0.0884	0.0670	
Mean	0.2361			0.1801	0.0875	0.0668	
ICRP66 →				0.217	0.173		

**Table 6.** Absorbed fraction for basal cell nuclei and layers in BB region.

Source		Ge. No ↓	Layer		Nuclei	
			6 MeV	7.69 MeV	6 MeV	7.69 MeV
Fast mucus	This work	1	$2.50 \times 10^{-3}$	0.0729	$5.91 \times 10^{-4}$	0.0177
		2	$2.49 \times 10^{-3}$	0.0745	$6.01 \times 10^{-4}$	0.0179
		3	$2.48 \times 10^{-3}$	0.0747	$6.09 \times 10^{-4}$	0.0183
		4	$2.48 \times 10^{-3}$	0.0754	$6.14 \times 10^{-4}$	0.0181
		5	$2.52 \times 10^{-3}$	0.0760	$6.02 \times 10^{-4}$	0.0183
		6	$2.47 \times 10^{-3}$	0.0761	$6.55 \times 10^{-4}$	0.0187
		7	$2.46 \times 10^{-3}$	0.0766	$6.62 \times 10^{-4}$	0.0187
		8	$3.82 \times 10^{-3}$	0.0782	$1.03 \times 10^{-4}$	0.0195
		Mean	$2.65 \times 10^{-3}$	0.0755	$6.71 \times 10^{-4}$	0.0184
		ICRP66 →		$5 \times 10^{-3}$	0.0893	
Slow mucus		Ge. No ↓				
		1	$1.36 \times 10^{-2}$	0.0776	$3.33 \times 10^{-3}$	0.0187
		2	$1.04 \times 10^{-2}$	0.0597	$3.23 \times 10^{-3}$	0.0189
		3	$1.36 \times 10^{-2}$	0.0788	$3.38 \times 10^{-3}$	0.0193
		4	$1.37 \times 10^{-2}$	0.0794	$3.29 \times 10^{-3}$	0.0191
		5	$1.38 \times 10^{-2}$	0.0799	$3.30 \times 10^{-3}$	0.0194
		6	$1.36 \times 10^{-2}$	0.0801	$3.48 \times 10^{-3}$	0.0196
		7	$1.37 \times 10^{-2}$	0.0805	$3.42 \times 10^{-3}$	0.0196
		8	$1.65 \times 10^{-2}$	0.0788	$4.31 \times 10^{-3}$	0.0196
		Mean	0.0136	0.0768	$3.47 \times 10^{-3}$	0.0193
ICRP66 →		0.0217	0.0857			

**Table 7.** Specific energy in target cell nuclei (BB region).

Source	Ge. No ↓	Secretory cells		Basal cells	
		6 MeV	7.69 MeV	6 MeV	7.69 MeV
Fast mucus	1	144.22	292.02	1.49	56.96
	2	147.27	297.19	1.51	57.61
	3	147.12	298.40	1.53	58.91
	4	149.78	300.56	1.54	58.41
	5	150.78	300.88	1.51	59.12
	6	148.08	298.16	1.65	60.36
	7	150.16	298.84	1.67	60.13
	8	146.92	296.20	2.60	62.80
	Mean	148.04	297.78	1.69	59.29
Slow mucus	1	173.62	303.75	8.38	60.40
	2	174.82	309.03	8.14	60.87
	3	174.27	308.78	8.50	62.19
	4	174.92	310.19	8.29	61.67
	5	177.84	311.74	8.30	62.41
	6	173.55	309.63	8.76	63.14
	7	174.64	268.04	8.61	63.12
	8	172.19	307.78	10.85	63.18
	Mean	174.48	303.62	8.73	62.12

## CONCLUSION

Absorbed fraction and specific energy from alpha particles emitted by radon progeny in airway tube for a Syrian adult man were calculated using Micro-dosimetry approach. A combination between Solidworks software and MCNPX code was used to construct the geometry. Comparisons with ICRP66 AFs data indicate the influence of geometry and target cells distribution on absorbed fraction and specific energy values. The present work shows that the determination of absorbed fraction of alpha particles can be a crucial factor in calculating other quantities such as the dose conversion factor. Furthermore, ICRP66 assumes equal importance of doses and thus equal sensitivities for basal and secretory cells. According to results presented in this study this weighting scheme might need to be reviewed. Based on results presented here the effective doses and dose conversion factors from short-lived radon progeny can be calculated when other exposure parameters are known.

**Table 8.** Specific energy in target cell nuclei (bb region).

Source	Ge. No ↓	Specific energy (mGy)			
		Fast mucus		Slow mucus	
		6 MeV	7.69 MeV	6 MeV	7.69 MeV
	9	296.82	286.24	312.68	296.92
	10	272.67	275.39	286.57	285.11
	11	262.84	264.82	275.43	273.35
	12	314.23	314.97	329.85	324.87
	13	316.65	315.96	330.59	325.14
	14	328.44	324.55	341.99	334.09
	15	305.90	299.56	316.65	307.36
	Mean	299.65	297.36	313.39	306.69

**Conflicts of interest:** Declared none.

## REFERENCES

- Krstic D, Nikezic D, Markovic VM, Vucic D (2013) Absorbed fractions in sensitive regions of human respiratory tract calculated by MCNP5/X software for electron and beta particles due to radon progeny. *Rom J Phys*, **58**: 164-171.
- Angeles A and Espinosa G (2011) Study of deposited energy in lung tissue from radon's progeny calculated by Monte Carlo. *Rev Mex Fis*, **57(1)**: 97-101.
- Leonard BE, Thompson RE, Beecher GC (2011) Human lung cancer risks from radon - part I - influence from bystander effects - a microdose analysis. *Dose Response*, **9(2)**: 243-92.
- Balázs G Madas (2016) Radon induced hyperplasia: effective adaptation reducing the
- local doses in the bronchial epithelium. *J Radiol Prot*, **36(3)**: 653-666.
- Farkas A, Hofmann W, Balásházy I, Szoke I, Madas BG, Moustafa M (2011) Effect of site-specific bronchial radon progeny deposition on the spatial and temporal distributions of cellular responses. *Radiat Environ Biophys*, **50(2)**: 281-97.
- Yu KN, Lau BMF, Nikezic D (2006) Assessment of environmental radon hazard using human respiratory tract mod-

- els. *J Hazard Mater*, **132(1)**: 98-110.
8. International Commission on Radiological Protection ICRP (1994) Human respiratory tract model for radiological protection. ICRP Publication 66, Pergamon Press, Oxford.
  9. Nikezic D, Lau BM, Stevanovic N, Yu KN (2006) Absorbed dose in target cell nuclei and dose conversion coefficient of radon progeny in the human lung. *J Environ Radioact*, **89(1)**: 18-29.
  10. Nikezic D and Yu KN (2001) Microdosimetric calculation of absorption fraction and the resulting dose conversion factor for radon progeny. *Radiat Environ Biophys*, **40(3)**: 207-211.
  11. Hofmann W, Fakir H, Aubineau-Laniece I, Pihet P (2004) Interaction of alpha particles at the cellular level implications for the radiation weighting factor. *Radiat Prot Dosimetry*, **112(4)**: 493-500.
  12. Lia WB, Hofmann W, Friedland W (2018) Microdosimetry and nanodosimetry for internal emitters. *Radiat Meas*, **115**: 29-42.
  13. Hui TE, Poston JW, Fisher DR (1990) The Microdosimetry of radon decay products in the respiratory tract. *Radiat Prot Dosimetry*, **31(1-4)**: 405-411.
  14. Katz R and Hofmann W (1982) Biological effects of low doses of ionising radiations: particle tracks in radiobiology. *Nucl Instrum Methods*, **203(1-3)**: 433-442.
  15. Hofmann W, Heistracher T, Caswell RS, Karam LR (1996) Track structure predictions of radon-induced biological effects in human bronchial epithelium. *Environ Int*, **22**: 949-957.
  16. Sedláč A (1996) Microdosimetric approach to the problem of lung cancer induced by radon progenies. *Health Phys*, **70(5)**: 680-8.
  17. Miller RC, Richard M, Brenner DJ, Hall EJ, Jostes R, Hui TE, Brooks AL (1996) Comparison of oncogenic transformation by accelerator produced monoenergetic alpha particles and by polyenergetic alpha particles from radon progeny. *Radiat Res*, **146**: 75-80.
  18. Caswell RS and Coyne JJ (1990) Microdosimetry of radon and radon daughters. *Rad Prot Dosim*, **31(1-4)**: 395-398.
  19. Hofmann W, Ménache MG, Crawford Brown DJ, Caswell RS, Karam LR (2000) Modelling energy deposition and cellular radiation effects in human bronchial epithelium by radon progeny alpha particles. *Health Phys*, **78**: 377-393.
  20. Nikezic D, Haque AK, Yu KN (2002) Absorbed dose delivered by alpha particles calculated in cylindrical geometry. *J Environ Radioact*, **60(3)**: 293-305.
  21. Fakir H, Hofmann W, Aubineau Laniece I (2006) Modelling the effect of non-uniform radon progeny activities on transformation frequencies in human bronchial airways. *Rad Prot Dosim*, **121**: 221-235.
  22. Lau BMF, Nikezic D, Yu KN (2007) Microdosimetry calculation of the dose conversion coefficient for radon progeny. IRPA, International Radiation Protection Association. Available at: <http://irpa11.irpa.net/pdfs/3g22.pdf>.
  23. National Research Council NRC (1991) Comparative dosimetry of radon in mines and homes. Washington D C: National Academy Press.
  24. Taleb B, Khadour A, Bitar A (2015) Reconstruction of head-to-knee voxel model for Syrian adult male of average height and weight. *EJRNMM*, **46(2)**: 491-497.
  25. 3D Slicer Free Open Source Software (BSD-style license), Version 4.7.0. Available at: <https://www.slicer.org/>.
  26. SolidWorks Corporation, Massachusetts Institute of Technology, USA. Solidworks Premium x64bit Service Pack version 15.0. Available at: <https://www.solidworks.com/>.
  27. Nikezic D, Yu KN, Cheung TTK, Haque AK MM, Vucic D (2000) Effects of different lung morphometry models on the calculated dose conversion factor from Rn progeny. *J Environ Radioact*, **47**: 263-277.
  28. Mercer RR, Russell ML, Crapo JD (1991) Radon dosimetry based on the depth distribution of nuclei in human and rat lungs. *Health Phys*, **61**: 117-130.
  29. Szóke I, Farkas Á, Balásházy I, Hofmann W (2008) Modelling of cell deaths and cell transformations of inhaled radon in homes and mines based on a biophysical and microdosimetric model. *Int J Radiat Biol*, **84(2)**: 127-138.
  30. De Vera P, Surdutovich E, Abril I, Garcia-Molina R, Solov'yov AV (2014) Analytical model of ionization and energy deposition by proton beams in subcellular compartments. *Eur Phys J*, **68(4)**: 96.1-96.8.
  31. International Commission of Radiation Units and Measurements ICRU (1993) Stopping powers and ranges for protons and alpha particles. ICRU Report 49, Maryland.
  32. Byrne HL, McNamara AL, Domanova W, Guatelli S, Kuncic Z (2013) Radiation damage on sub-cellular scales: beyond DNA. *Phys Med Biol*, **58(5)**: 1251-67.
  33. John S Hendricks and the MCNPX Team (2002) MCNPX Version 2.5.B. Los Alamos
  34. National Laboratory report LA-UR-02-7086.
  35. Ansys Inc (2013) Design Modeler User Guide. Release 15.
  36. Lazarine Alexis D (2006) Medical physics calculations with MCNP™: a primer. Master thesis in health physics. Texas A&M University, USA.
  37. Nikezic D, Novakovic B, Yu KN (2003) Absorbed fraction of radon progeny in human bronchial airways with bifurcation geometry. *Int J Radiat Biol*, **79(3)**: 175-180.
  38. Nikezic D, Yu KN, Vucic D (2001) Absorbed fraction and dose conversion coefficients of alpha particles for radon dosimetry. *Phys Med Biol*, **46**: 1963-1974.
  39. Yuness M, Mohamed A, Abd El-hady M, Moustafa M, Nazmy H (2015) Effect of indoor activity size distribution of <sup>222</sup>Rn progeny in-depth dose estimation. *Appl Radiat Isot*, **97**: 34-39.

